

Cosmic Tidal Reconstruction

Hong-Ming Zhu,^{1,2} Ue-Li Pen,^{3,4,5} Yu Yu,⁶ Xinzhong Er,^{1,7} and Xuelei Chen^{1,2,8}

¹*Key Laboratory for Computational Astrophysics, National Astronomical Observatories, Chinese Academy of Sciences, 20A Datun Road, Beijing 100012, China*

²*University of Chinese Academy of Sciences, Beijing 100049, China*

³*Canadian Institute for Theoretical Astrophysics, 60 St. George Street, Toronto, ON M5S 3H8, Canada*

⁴*Canadian Institute for Advanced Research, CIFAR Program in Gravitation and Cosmology, Toronto, ON M5G 1Z8, Canada*

⁵*Perimeter Institute for Theoretical Physics, 31 Caroline St. N., Waterloo, ON, N2L 2Y5, Canada*

⁶*Key laboratory for research in galaxies and cosmology, Shanghai Astronomical Observatory, Chinese Academy of Sciences, 80 Nandan Road, Shanghai 200030, China*

⁷*INAF, Osservatorio Astronomico di Roma, via Frascati 33, I-00040, Monteporzio Catone, Italy*

⁸*Center of High Energy Physics, Peking University, Beijing 100871, China*

(Dated: May 13, 2019)

The gravitational coupling of a long wavelength tidal field with small scale density fluctuations leads to anisotropic distortions of the locally measured small scale matter correlation function. Since the local correlation function is statistically isotropic in the absence of such tidal interactions, the tidal distortions can be used to reconstruct the long wavelength tidal field and large scale density field in analogy with the cosmic microwave background lensing reconstruction. In this paper we present in detail a formalism for the cosmic tidal reconstruction and test the reconstruction in numerical simulations. We find that the density field on large scales can be reconstructed with good accuracy and the cross correlation coefficient between the reconstructed density field and the original density field is greater than 0.9 on large scales ($k \lesssim 0.1h/\text{Mpc}$). This is useful in the 21cm intensity mapping survey, where the long wavelength radial modes are lost due to foreground subtraction process.

PACS numbers:

I. INTRODUCTION

The large scale structure contains a wealth of information about our Universe. The cosmic acceleration, neutrino masses, early universe models and other properties of the Universe can be inferred with current or upcoming surveys. The initially linear and Gaussian density perturbations grow due to gravitational interaction, the nonlinearities develop and induce the couplings between different modes. This leads to striking non-Gaussian features in the large scale structure of the Universe, limiting the cosmological information that can be extracted from galaxy surveys. At the same time, however, such correlations between the different perturbation modes on different scales also imply that we could infer information about the large scale density field by observing small scale density fluctuations.

The basic idea is that the evolution of small scale density perturbations $\delta(\mathbf{k}_S)$ is modulated by long wavelength perturbations Φ_L , causing both isotropic and anisotropic distortions of the local small scale power spectrum [1]. The isotropic distortion, which only depends on the magnitude of the wavenumber \mathbf{k}_S , is mainly due to the change in the background density from the long wavelength density perturbation $\nabla^2\Phi_L \propto \delta_L$, where Φ_L denotes the long wavelength gravitational potential. The anisotropic distortion, which also depends on the direction of \mathbf{k}_S , is induced by the long wavelength tidal field $t_{ij} = \Phi_{L,ij} - \delta_{ij}\nabla^2\Phi_L/3$, where $\Phi_{L,ij} \equiv \partial^2\Phi_L/\partial x^i\partial x^j$. Using the isotropic modulation on the small scale power spectrum to reconstruct the large scale density field has

been studied in Ref.[2]. However, the anisotropic distortions are more robust, since many other processes can also lead to isotropic distortions in the local small scale power spectrum. By applying quadratic estimators which quantify the local anisotropy of small scale density statistics, the long wavelength tidal field can be reconstructed accurately [3]. In general, this method can obtain measurement of long wavelength modes with better precision, this is especially valuable when these modes can not be obtained directly. The reconstruction of the long wavelength tidal field from the local small scale power spectrum is similar to the reconstruction of shear fields in gravitational lensing [4, 5].

In this paper we present the cosmic tidal reconstruction method in detail. The evolution of small scale density fluctuations in the presence of the long wavelength tidal field t_{ij} has been studied extensively in Ref.[1]. The tidal distortion of the local small scale power spectrum is given by

$$\delta P(\mathbf{k}_S, \tau)|_{t_{ij}} = \hat{k}_S^i \hat{k}_S^j t_{ij}^{(0)} P_{1s}(k_S, \tau) f(k_S, k_L, \tau), \quad (1)$$

where $\hat{\mathbf{k}}$ denotes the unit vector in the direction of \mathbf{k} , $P_{1s}(k_S, \tau)$ is the isotropic linear power spectrum, $f(k_S, k_L, \tau)$ describes the coupling of the long wavelength tidal field to the small scale density fluctuations and superscript (0) denotes some “initial” time. The anisotropic distortion can be decomposed into several orthogonal quadrupolar distortions as in weak lensing. While t_{ij} in principle has 5 independently observable components, in this paper we shall focus on the two trans-

verse shear terms, $(\hat{k}_1^2 - \hat{k}_2^2)\gamma_1^{(0)}P_{1s}f$ and $2\hat{k}_1\hat{k}_2\gamma_2^{(0)}P_{1s}f$, which describe orthogonal quadrupolar distortions in the tangential plane perpendicular to the line of sight. Here $\gamma_1 = (\Phi_{L,11} - \Phi_{L,22})/2$ and $\gamma_2 = \Phi_{L,12}$. The quadrupolar distortions containing \hat{k}_3 will be affected by peculiar velocities, and require additional treatments beyond the scope of this paper. These two tidal shear fields γ_1 and γ_2 can be converted into the 2D convergence field, $\kappa_{2D} \equiv (\Phi_{L,11} + \Phi_{L,22})/2$, using the relation

$$\kappa_{2D,11} + \kappa_{2D,22} = \gamma_{1,11} - \gamma_{1,22} + 2\gamma_{2,12}. \quad (2)$$

We can obtain the 3D convergence field $\kappa_{3D} \equiv \nabla^2\Phi_L/3$ from the 2D convergence by the relation

$$\kappa_{3D,11} + \kappa_{3D,22} = \frac{2}{3}\nabla^2\kappa_{2D}. \quad (3)$$

The large scale density field δ_L is then given by the 3D convergence field through the Poisson equation. The transverse shear fields are evaluated by applying quadratic estimators to the density field as in weak lensing. The optimal tidal shear estimators can be derived under the Gaussian assumption.

We call this method *cosmic tidal reconstruction*, as it exploits the local anisotropic features from tidal interactions. Each independent measurement of the small scale power spectrum gives some information about the power spectrum on large scales. Thus instead of being limited by the non-Gaussianity on small scales, we exploit these strong correlations to improve the measurement of the large scale structure.

Since we only use the tidal shear fields in the $x - y$ plane to reconstruct the long wavelength density field, the changes of long wavelength density field δ_L along z axis is inferred from the variations of tidal shear fields γ_1 and γ_2 along z axis. We can not capture rapid changes of the density field along z axis, i.e. those modes with large k_{\parallel} . This is reflected by the anisotropic noise of the reconstructed mode $\kappa_{3D}(\mathbf{k})$, which is $\sigma_{\kappa_{3D}}^2 \propto (k^2/k_{\perp}^2)^2$ (see Sec.III for derivation). The noise is infinite when $k_{\perp} \rightarrow 0$. In this case, we expect these modes contain nothing but noise. The well reconstructed modes are those with small k_{\parallel} and large k_{\perp} . This is useful in the cross correlation of 21cm intensity mapping survey with other cosmic probes such as ISW, lensing, photo- z galaxies, optical depth, and others [6, 7]. These low k_{\parallel} modes are normally lost in the 21cm intensity mapping data due to foreground subtraction process [8].

The local quadrupolar distortions have also been discussed in [9, 10] where the theoretical constructions were outlined. The basic idea of purely transverse tidal reconstruction has been studied in Ref.[3]. This paper expands on the early work by considering the tidal reconstruction method in detail. This paper is organized as follows. In Section II, we present the basic formalism, including the kinematics and dynamics. In Section III we construct the tidal shear estimators and present the reconstruction algorithm. In Section IV, we study the tidal reconstruction by using N -body simulation data. In Section V, we

examine the validity of cosmic tidal reconstruction and discuss its future applications.

II. TIDAL DEFORMATION

The motion of a dark matter fluid element in the Universe includes translation, rotation and deformation. Let us consider two neighboring points P_0 and P in the fluid at time t_0 , the velocity $\mathbf{v}|_P$ can be expanded as

$$v^i|_P = v^i|_{P_0} + (S^i_j + A^i_j)|_{P_0}\Delta x^j. \quad (4)$$

The symmetric part $S^i_j = (v^i_{,j} + v^j_{,i})/2$ is the deformation velocity tensor in fluid mechanics, with diagonal components describing the stretching along three axes and off-diagonal components describing the shear motion. The anti-symmetry part $A^i_j = (v^i_{,j} - v^j_{,i})/2$ describes the rotation of this fluid element. In the free falling reference system of this fluid element, $v|_{P_0} = 0$, with P_0 as the origin point. Neglecting the rotation, the position of P at time t is given by

$$x^i(t)|_P = x^i + \int_{t_0}^t S^i_j(t')|_{P_0} dt' x^j, \quad (5)$$

where $x^i = \Delta x^i$ is the initial separation between P_0 and P . The shape tensor $\mathfrak{S}^i_j = \int_{t_0}^t S^i_j(t')|_{P_0} dt'$ describes the deformation. In the local inertial frame, the dark matter fluid element is only sensitive to the residual anisotropy of gravitational forces, which causes the fluid element to deform. A dark matter fluid element deforms under the gravitational interaction between this fluid element and surrounding large scale structures if the gravitational interaction between different smaller parts of this fluid element can be neglected. It is the same as ocean tides on the Earth induced by the tidal forces from the Moon and the Sun. We call such effects induced by the surrounding large scale structure *cosmic tides* [3]. By observing these local anisotropies, we can measure the large scale tidal field and density field. In reality, the interaction between a long wavelength tidal field and small scale density fluctuations is more complicated than the displacement of particles in a fluid element, we shall discuss this in more detail below.

The effect of a general long wavelength tidal field on the evolution of small scale density perturbations with $k_L \ll k_S$ has been studied in [1]. Here we focus on the effect of the traceless tidal field $t_{ij} = \Phi_{L,ij} - \delta_{ij}\nabla^2\Phi_L/3$ from a long wavelength scalar perturbation Φ_L .

In the expanding universe, the equation of motion for a particle is

$$\frac{d^2\mathbf{x}}{d\tau} + \mathcal{H}(\tau)\frac{d\mathbf{x}}{d\tau} = -\nabla_{\mathbf{x}}\phi, \quad (6)$$

where \mathbf{x} is the comoving Eulerian coordinate, τ is the conformal time, $\mathcal{H}(\tau) = d\ln a/d\tau$ is the comoving Hubble

parameter, $a(\tau)$ is the scale factor and ϕ is the gravitational potential. In Lagrangian perturbation theory, the dynamical variable is the Lagrangian displacement field $\mathbf{s}(\mathbf{q}, \tau)$, defined as

$$\mathbf{x}(\mathbf{q}, \tau) = \mathbf{q} + \mathbf{s}(\mathbf{q}, \tau), \quad (7)$$

where \mathbf{q} is the comoving Lagrangian coordinate. The displacement field maps the initial particle position \mathbf{q} into the final Eulerian position \mathbf{x} . The density contrast $\delta(\mathbf{x})$ is given by the mass conservation relation:

$$\delta(\mathbf{x}(\mathbf{q}, \tau)) = \frac{1}{J(\mathbf{q}, \tau)} - 1, \quad (8)$$

where $J(\mathbf{q}, \tau) = \det(\delta^i_j + M^i_j(\mathbf{q}, \tau))$ and $M^i_j = \partial s^i / \partial q^j$.

To study the evolution of small scale density perturbations in the presence of the long wavelength tidal field, the gravitational potential ϕ in Eq.(6), which drives the motion of a particle, contains not only the part sourced by the small scale density fluctuations, Φ_s , but also a part induced by the long wavelength tidal field [1],

$$\phi(\mathbf{x}(\mathbf{q}, \tau)) = \Phi_s(\mathbf{x}(\mathbf{q}, \tau)) + \frac{1}{2} t_{ij}(\mathbf{0}, \tau) x^i x^j + \dots \quad (9)$$

The tidal field can be written as $t_{ij}(\mathbf{0}, \tau) = T(\tau) t_{ij}^{(0)}(\mathbf{0})$, where superscript (0) denotes the tidal field evaluated at the “initial” time τ_0 , $T(\tau) = D(\tau)/a(\tau)$ is the linear transfer function, $D(\tau)$ is the linear growth function, and $D(\tau_0) = a(\tau_0) = 1$. Note that at the origin of the free falling frame, the contribution from the tidal field is by definition zero. The small scale potential Φ_s satisfies the Poisson equation,

$$\nabla^2 \Phi_s = 4\pi G a^2 \bar{\rho} \delta = \frac{3}{2} \Omega_m(\tau) \mathcal{H}^2 \delta, \quad (10)$$

where $\Omega_m(\tau)$ is the density parameter at τ .

The above equations can be solved perturbatively. We decompose the displacement as

$$\mathbf{s} = \mathbf{s}_s + \mathbf{s}_t, \quad (11)$$

where \mathbf{s}_s and \mathbf{s}_t are the contributions from the small scale potential and long wavelength tidal field respectively. Then $M^i_j = M_s^i_j + M_t^i_j$ with $M_s^i_j = \partial s_s^i / \partial q^j$ and $M_t^i_j = \partial s_t^i / \partial q^j$. Here we only consider the linear displacement \mathbf{s}_{1s} , \mathbf{s}_{1t} and the quadratic term \mathbf{s}_{2t} from the coupling of \mathbf{s}_{1s} and \mathbf{s}_{1t} , and neglect the terms of order $(\mathbf{s}_{1s})^2$. In the follow calculations, we focus on the coupling between the long mode (large scale tidal field) and the short mode (small scale density field), assuming that both large and small scale density fields follow linear evolutions.

At linear order, Eq.(6) becomes two equations for \mathbf{s}_{1s} and \mathbf{s}_{1t} , respectively,

$$\left[\frac{d^2}{d\tau^2} + \mathcal{H} \frac{d}{d\tau} \right] s_{1s}^i(\mathbf{q}, \tau) = -\partial_q^i \Phi_{1s}(\mathbf{q}, \tau), \quad (12)$$

$$\left[\frac{d^2}{d\tau^2} + \mathcal{H} \frac{d}{d\tau} \right] s_{1t}^i(\mathbf{q}, \tau) = -\frac{1}{2} \partial_q^i [t_{kl}(\tau) q^k q^l], \quad (13)$$

where $\partial_q^i \equiv \delta^{ij} \partial / \partial q^j$, $\nabla_q^2 \Phi_{1s} = 3\Omega_m(\tau) \mathcal{H}^2 \delta_{1s} / 2$ and $\delta_{1s} = -s_{1s,i}^i$. Eq.(12) can be solved to get

$$s_{1s}^i(\mathbf{q}, \tau) = -\frac{\partial_q^i}{\nabla_q^2} \delta_{1s}(\mathbf{q}, \tau) = -D(\tau) \frac{\partial_q^i}{\nabla_q^2} \delta_{1s}(\mathbf{q}, \tau_0). \quad (14)$$

The operator $1/\nabla^2$ denotes the inverse operator for ∇^2 , which can be easily computed in Fourier space. Eq.(13) describes the evolution of the displacement induced by the long wavelength tidal field, and can be integrated to get

$$s_{1t}^i(\mathbf{q}, \tau) = -F(\tau) t^{(0)i}_j q^j, \quad (15)$$

where

$$F(\tau) = \int_0^\tau d\tau'' a(\tau'') T(\tau'') G(\tau - \tau''), \quad (16)$$

and $G(\tau - \tau'') = \int_{\tau''}^\tau d\tau' / a(\tau')$. The induced linear density fluctuation δ_{1t} is given by

$$\delta_{1t} = -s_{1t,i}^i = F(\tau) t^{(0)i}_i. \quad (17)$$

The trace of the tidal field t_{ij} is zero, i.e. $\delta_{1t} = 0$, so there is no first order contribution to the density from the tidal field.

The evolution equation for \mathbf{s}_{2t} involves quadratic mixed terms from the coupling between \mathbf{s}_{1s} and \mathbf{s}_{1t} . Inserting the Poisson equation to Eq.(6), and subtracting the evolution equations for \mathbf{s}_{1s} , \mathbf{s}_{1t} and \mathbf{s}_{2s} leads to

$$\begin{aligned} & \frac{d^2}{d\tau^2} \sigma_{2t} + \mathcal{H} \frac{d}{d\tau} \sigma_{2t} - \frac{3}{2} \Omega_m(\tau) \mathcal{H}^2 \sigma_{2t} \\ &= -\frac{3}{2} \Omega_m(\tau) \mathcal{H}^2 \delta_{1s} \delta_{1t} + \left(\frac{\partial^i \partial^j}{\nabla^2} \delta_{1s} \right) t_{ij}(\tau), \end{aligned} \quad (18)$$

where $\sigma \equiv s^i_{,i}$. Note that at linear order, M_{1t} should not be included when expanding Eq.(10), as it is induced by the long wavelength tidal field t_{ij} , while the coupling between M_{1s} and M_{1t} should be included when expanding to second order as they source the local gravitational potential Φ_s . The first term on the right hand of Eq.(18) vanishes since $\delta_{1t} = 0$. This equation can be solved numerically to get

$$\sigma_{2t}(\mathbf{q}, \tau) = D_{\sigma 1}(\tau) \left(\frac{\partial^i \partial^j}{\nabla^2} \delta_{1s}(\mathbf{q}, \tau) \right) t_{ij}^{(0)}, \quad (19)$$

where

$$D_{\sigma 1}(\tau) = \int_0^\tau d\tau' \frac{H(\tau) D(\tau') - H(\tau') D(\tau)}{\dot{H}(\tau') D(\tau') - H(\tau') \dot{D}(\tau')} \frac{T(\tau') D(\tau')}{D(\tau)}. \quad (20)$$

The difference between density contrasts with and without t_{ij} at \mathbf{x} is

$$\delta_t(\mathbf{x}) = \delta(\mathbf{x}) - \delta(\mathbf{x})|_{t_{ij}=0}. \quad (21)$$

Since the tidal field induces the displacement \mathbf{s}_t in addition to \mathbf{s}_s , the same Lagrangian coordinate \mathbf{q} corresponds

to different \mathbf{x} in these two cases. In the presence of t_{ij} , $\mathbf{x} = \mathbf{q} + \mathbf{s}_{1s} + \mathbf{s}_{1t}$. Here δ_{1s} solved from linear equations gives the density at $\mathbf{x}_s = \mathbf{q} + \mathbf{s}_{1s} = \mathbf{x} - \mathbf{s}_{1t}$. Taking this into account and using Eq.(8), we finally obtain

$$\delta_t(\mathbf{x}) = \delta_{1t}(\mathbf{x}) - \sigma_{2t}(\mathbf{x}) + \delta_{1t}(\mathbf{x})\delta_{1s}(\mathbf{x}) + \text{tr}(\mathbf{M}_{1s}\mathbf{M}_{1t})|_{\mathbf{x}} - s_{1t}^i \partial_i \delta_{1s}(\mathbf{x}). \quad (22)$$

Inserting the first and second order solutions and noting that the tidal field is traceless, we obtain the anisotropic small scale density fluctuations induced by the long wavelength tidal field t_{ij} :

$$\delta_t(\mathbf{x}, \tau) = t_{ij}^{(0)} \left[\alpha(\tau) \frac{\partial^i \partial^j}{\nabla^2} + \beta(\tau) x^i \partial^j \right] \delta_{1s}(\mathbf{x}, \tau), \quad (23)$$

where $\alpha(\tau) = -D_{\sigma 1}(\tau) + F(\tau)$ and $\beta(\tau) = F(\tau)$.

In the above we have used the linear density-displacement relation $\delta_{1s} = -s_{1s,i}^i$ to convert the linear displacement field \mathbf{s}_{1s} to the small scale density field δ_{1s} . However, the linear relation does not hold well at low redshifts and small scales [11]. While the logarithmic relation between the divergence of the displacement field and the density field,

$$s_{1s,i}^i = -\ln(1 + \delta_{1s}) + \langle \ln(1 + \delta_{1s}) \rangle, \quad (24)$$

is much tighter and straighter at low redshifts and small scales[11]. Below we will use the logarithmic variable $\delta_g = \ln(1 + \delta_{1s})$ in place of δ_{1s} in the reconstruction. This logarithmic transform reduces non-Gaussianities in the density field, hence improves the reconstruction [3].

The tidal field t_{ij} with wavenumber k_L can be taken as constant in a small patch with scale $\ll 1/k_L$. Note it is different to have a constant tidal field t_{ij} and a constant gravitational field Φ_L . The former corresponds to the second spatial derivative of the latter. The local correlation function in the free falling frame is

$$\xi(\mathbf{r}, \tau) = \langle \delta(\mathbf{0}, \tau) \delta(\mathbf{r}, \tau) \rangle, \quad (25)$$

where $\delta = \delta_{1s} + \delta_t$. Using Eq.(23), we obtain

$$\xi(\mathbf{r}, \tau) = \xi_{1s}(r, \tau) + t_{ij}^{(0)} \left[2\alpha(\tau) \frac{\partial^i \partial^j}{\nabla^2} + \beta(\tau) r^i \partial^j \right] \xi_{1s}(r, \tau), \quad (26)$$

where $\xi_{1s}(r, \tau) = \langle \delta_{1s}(\mathbf{0}, \tau) \delta_{1s}(\mathbf{r}, \tau) \rangle$ is the isotropic linear matter correlation function. The anisotropic distortion of the locally measured small scale density correlation function is induced by the long wavelength tidal field t_{ij} . Transforming Eq.(26) to Fourier space, we get the local small scale power spectrum,

$$P(\mathbf{k}, \tau)|_{t_{ij}} = P_{1s}(k, \tau) + \hat{k}^i \hat{k}^j t_{ij}^{(0)} P_{1s}(k, \tau) f(k, \tau), \quad (27)$$

where $P_{1s}(k, \tau)$ is the isotropic linear power spectrum, and

$$f(k, \tau) = 2\alpha(\tau) - \beta(\tau) \frac{d \ln P_{1s}(k, \tau)}{d \ln k}. \quad (28)$$

Here we abbreviate k_S as k and suppress the argument k_L since $T(\tau)$ is scale independent.

III. TIDAL RECONSTRUCTION

In this section we first construct the tidal shear estimators, then present the algorithm for density reconstruction.

A. Tidal Shear Estimators

We first construct the unbiased minimum variance tidal shear estimators in the long wavelength limit, where γ_1 and γ_2 are constant in space, then generalize the estimators to the spatial varying case. We also discuss what happens when the long wavelength limit does not hold.

In the long wavelength limit and under the Gaussian assumption, quadratic estimators can be constructed either by using the maximum likelihood method[4] or the inverse variance weighting [5, 12],

$$\hat{\gamma}_1 = \frac{1}{Q_{\gamma_1}} \int \frac{d^3 k}{(2\pi)^3} \frac{|\delta_g(\mathbf{k})|^2}{L^3} \frac{P(k)}{P_{\text{tot}}^2(k)} f(k) (\hat{k}_1^2 - \hat{k}_2^2), \quad (29)$$

$$\hat{\gamma}_2 = \frac{1}{Q_{\gamma_2}} \int \frac{d^3 k}{(2\pi)^3} \frac{|\delta_g(\mathbf{k})|^2}{L^3} \frac{P(k)}{P_{\text{tot}}^2(k)} f(k) (2\hat{k}_1 \hat{k}_2), \quad (30)$$

where $P_{\text{tot}}(k) = P(k) + P_N(k)$ is the observed power spectrum, including both the signal and noise, and

$$Q_{\gamma_1} = \int \frac{d^3 k}{(2\pi)^3} \frac{P^2(k)}{P_{\text{tot}}^2(k)} f^2(k) (\hat{k}_1^2 - \hat{k}_2^2)^2, \quad (31)$$

$$Q_{\gamma_2} = \int \frac{d^3 k}{(2\pi)^3} \frac{P^2(k)}{P_{\text{tot}}^2(k)} f^2(k) (2\hat{k}_1 \hat{k}_2)^2. \quad (32)$$

After integrating over angles in Fourier space, we have

$$Q_{\gamma_1} = Q_{\gamma_2} = Q = \int \frac{2k^2 dk}{15\pi^2} \frac{P^2(k)}{P_{\text{tot}}^2(k)} f^2(k) \quad (33)$$

Using Parseval's theorem, we can rewrite the above equations in real space,

$$\hat{\gamma}_1 = \frac{1}{L^3} \int d^3 x [\delta_g^{w_1}(\mathbf{x}) \delta_g^{w_1}(\mathbf{x}) - \delta_g^{w_2}(\mathbf{x}) \delta_g^{w_2}(\mathbf{x})], \quad (34)$$

and

$$\hat{\gamma}_2 = \frac{1}{L^3} \int d^3 x [2\delta_g^{w_1}(\mathbf{x}) \delta_g^{w_2}(\mathbf{x})], \quad (35)$$

where $\delta_g^{w_1}(\mathbf{x})$ and $\delta_g^{w_2}(\mathbf{x})$ are two filtered density fields. In Fourier space, they are given by

$$\delta_g^{w_i}(\mathbf{k}) = \delta_g(\mathbf{k}) w_i(\mathbf{k}), \quad (36)$$

where

$$w_i(\mathbf{k}) = \left[\frac{P(k) f(k)}{Q P_{\text{tot}}^2(k)} \right]^{1/2} \hat{k}_i. \quad (37)$$

In deriving Eq.(34) and Eq.(35), we have assumed that the tidal shear field is constant in space. From the expressions for $\hat{\gamma}_1$ and $\hat{\gamma}_2$, we can see the terms in square brackets give estimates for γ_1 and γ_2 at the location \mathbf{x} , while the integral $\int d^3x/L^3$ averages the local value over the whole space L^3 . If the fluctuation of the tidal field t_{ij} changed on a larger scale than the filtering scale, we can use the localized estimation in the square brackets as estimates for γ_1, γ_2 [4, 5, 12]. The unbiased minimum variance estimates of the spatial varying tidal field in the long wavelength limit is given by

$$\begin{aligned}\hat{\gamma}_1(\mathbf{x}) &= [\delta_g^{w_1}(\mathbf{x})\delta_g^{w_1}(\mathbf{x}) - \delta_g^{w_2}(\mathbf{x})\delta_g^{w_2}(\mathbf{x})], \\ \hat{\gamma}_2(\mathbf{x}) &= [2\delta_g^{w_1}(\mathbf{x})\delta_g^{w_2}(\mathbf{x})].\end{aligned}\quad (38)$$

The estimators given in Eq.(38) were derived assuming that compared with the small scale density field, the long wavelength tidal shear fields vary slowly. If the long wavelength limit is not satisfied, the tidal shear reconstruction would be biased by a multiplicative bias factor $b(\mathbf{k})$, which approaches to unity in the limit $k \rightarrow 0$ and decreases when k increases [4, 12]. In the cosmic tidal reconstruction, we mainly use the nonlinear structures around the scale 1.25 Mpc/ h to reconstruct the long wavelength tidal field [3], so for the reconstructed large scale density perturbations with wavenumber $k_L \lesssim 0.1 h/\text{Mpc}$ we can ignore this multiplicative bias.

B. Density Reconstruction Algorithm

The symmetric 3×3 tensor $\Phi_{L,ij}$ can be decomposed into 6 independently observable components [10, 13], i.e. $\Phi_{L,ij} = A_a \epsilon_{ij}^a$, where A_a is the expansion coefficient and ϵ_{ij}^a satisfies the orthogonal relation $\epsilon_{ij}^a \epsilon^{bji} \propto \delta^{ab}$. We decompose $\Phi_{L,ij}$ as

$$\Phi_{L,ij} = (1 + \kappa_{3D})\delta_{ij} + t_{ij}, \quad (39)$$

where

$$t_{ij} = \begin{pmatrix} \gamma_1 - \gamma_z & \gamma_2 & \gamma_x \\ \gamma_2 & -\gamma_1 - \gamma_z & \gamma_y \\ \gamma_x & \gamma_y & 2\gamma_z \end{pmatrix}, \quad (40)$$

and $\gamma_1 = (\Phi_{L,11} - \Phi_{L,22})/2$, $\gamma_2 = \Phi_{L,12}$, $\gamma_x = \Phi_{L,13}$, $\gamma_y = \Phi_{L,23}$, $\gamma_z = (2\Phi_{L,33} - \Phi_{L,11} - \Phi_{L,22})/6$. The tensor is decomposed in a way such that when reduced to the 2D case, notations reduce to those used in gravitational lensing, so the z axis plays a different role than the x - and y -axes. For intuitive understandings of these abstract symbols, see the figures in Ref.[10]. All these 6 different components will induce different observable effects in the local quadratic statistics, including the isotropic modulations (κ_{3D}) and anisotropic parts (γ_1, γ_2 , etc). The large scale gravitational potential Φ_L is a single number, so it is six fold overdetermined. Using the isotropic modulation to reconstruct the large scale density field (super

sample signal) has been studied in [2]. Here we focus on the “change of shape”, i.e. the traceless tidal field $t_{ij} = \Phi_{L,ij} - \nabla^2 \Phi_L \delta_{ij}/3$ instead.

The induced local anisotropy pattern by long wavelength tidal field is proportional to t_{ij} . Using orthogonal components introduced above, Eq.(27) can be written as

$$\frac{\delta P(\mathbf{k}, \tau)|_{t_{ij}}}{P_{1s}(k, \tau)} = f(k, \tau)[(\hat{k}_1^2 - \hat{k}_2^2)\gamma_1^{(0)} + 2\hat{k}_1\hat{k}_2\gamma_2^{(0)}] + \dots \quad (41)$$

Here we only write out the γ_1 and γ_2 terms explicitly. The distortion along the line of sight (i.e. the z -direction in the above coordinates) is often affected by peculiar velocities in spectroscopic surveys, so here we shall use γ_1 and γ_2 which only involve derivatives in the tangential $x - y$ plane. In the language of weak lensing, γ_1 and γ_2 describe quadrupolar distortions in the $x - y$ plane. Peculiar velocities cause particles moving along z axis, but we expect the changes in γ_1 and γ_2 due to peculiar velocities to be a second order effect.

We can obtain the convergence field κ_{2D} from γ_1 and γ_2 as in gravitational lensing [14], $\kappa_{2D,11} + \kappa_{2D,22} = \gamma_{1,11} - \gamma_{1,22} + 2\gamma_{2,12}$. In Fourier space, the relation between the convergence and shear can be written as

$$\kappa_{2D}(\mathbf{k}) = \frac{1}{k_1^2 + k_2^2}[(k_1^2 - k_2^2)\gamma_1(\mathbf{k}) + 2k_1k_2\gamma_2(\mathbf{k})], \quad (42)$$

where we use the subscript 2D to indicate that κ_{2D} is the 2D convergence field in a constant redshift slice. It can be converted into the convergence field in three dimensional $\kappa_{3D} = \nabla^2 \Phi_L/3$ as

$$\begin{aligned}\kappa_{3D}(\mathbf{k}) &= \frac{2k^2}{3(k_1^2 + k_2^2)}\kappa_{2D}(\mathbf{k}) \\ &= \frac{2k^2}{3(k_1^2 + k_2^2)^2}[(k_1^2 - k_2^2)\gamma_1(\mathbf{k}) + 2k_1k_2\gamma_2(\mathbf{k})].\end{aligned}\quad (43)$$

Now we get an estimate of the large scale density field by measuring γ_1 and γ_2 . The large scale density field δ_L only differs from κ_{3D} by a constant factor which we will address in a moment.

Note that this reconstruction is inherently 3D instead of 2D. As only γ_1 and γ_2 are used, one might thought that the cosmic tidal reconstruction takes place in different 2D slices with constant redshifts. However, although γ_1 and γ_2 only involve derivatives in the tangential plane, the changes of γ_1 and γ_2 along z axis encode the change of δ_L along z axis. Since we only use γ_1 and γ_2 instead of all components in the tidal field t_{ij} for reconstruction, the error of the reconstructed mode $\kappa_{3D}(\mathbf{k})$ is anisotropic in \mathbf{k} . The variance of $\kappa_{3D}(\mathbf{k})$ is

$$\begin{aligned}\langle \kappa_{3D}(\mathbf{k})\kappa_{3D}(\mathbf{k}') \rangle &= [(k_1^2 - k_2^2)(k_1'^2 - k_2'^2)\langle \gamma_1(\mathbf{k})\gamma_1(\mathbf{k}') \rangle \\ &+ (2k_1k_2)(2k_1'k_2')\langle \gamma_2(\mathbf{k})\gamma_2(\mathbf{k}') \rangle] \times \frac{2k^2}{(k_\perp^2)^2} \frac{2k'^2}{(k_\perp'^2)^2},\end{aligned}\quad (44)$$

where $k_\perp = k_1^2 + k_2^2$. The power spectra of γ_1 and γ_2 are

scale independent on large scales [15], so

$$\begin{aligned} \langle \kappa_{3D}(\mathbf{k}) \kappa_{3D}(\mathbf{k}') \rangle &\propto [(k_1^2 - k_2^2)(k_1'^2 - k_2'^2) \\ &+ (2k_1 k_2)(2k_1' k_2')] \times \frac{2k^2}{(k_\perp^2)^2} \frac{2k'^2}{(k_\perp'^2)^2} \delta^D(\mathbf{k} + \mathbf{k}'), \end{aligned} \quad (45)$$

where $\delta^D(\mathbf{k})$ is the Dirac delta function. The error in the reconstructed mode $\kappa_{3D}(\mathbf{k})$ is $\sigma_{\kappa_{3D}}^2 \propto (k^2/k_\perp^2)^2$, which is anisotropic in k_\parallel and k_\perp . If we could include the z -components the error would be isotropic, but redshift space distortion will influence the reconstruction. We shall investigate this in the future.

We see that when $k_\perp \rightarrow 0$ the error is infinite for the corresponding $\kappa_{3D}(\mathbf{k})$. In this case, the estimator in Eq.(43) diverges. As these modes contain nothing but noise, we set these modes to zero in our reconstruction. Since the error varies for modes with different k_\perp and k_\parallel , we need to filter the reconstructed density field κ_{3D} to obtain the clean density field κ .

In general, the reconstructed noisy 3D convergence field κ_{3D} is related to the original density field by

$$\kappa_{3D}(k_\perp, k_\parallel) = b(k_\perp, k_\parallel) \delta_L(k_\perp, k_\parallel) + n(k_\perp, k_\parallel), \quad (46)$$

where $b(k_\perp, k_\parallel)$ is the bias factor and $n(k_\perp, k_\parallel)$ is the noise in reconstruction. The bias factor and the noise can be determined from the cross correlation of κ_{3D} and the original density field δ and the auto-correlation function of κ_{3D} ,

$$\langle \kappa_{3D} \delta \rangle = b \langle \delta \delta \rangle, \quad \langle \kappa_{3D} \kappa_{3D} \rangle = b^2 \langle \delta \delta \rangle + \langle nn \rangle. \quad (47)$$

We then get

$$b(k_\perp, k_\parallel) = \frac{P_{\kappa_{3D} \delta}(k_\perp, k_\parallel)}{P_\delta(k_\perp, k_\parallel)}, \quad (48)$$

$$P_n(k_\perp, k_\parallel) = P_{\kappa_{3D}}(k_\perp, k_\parallel) - b^2(k_\perp, k_\parallel) P_\delta(k_\perp, k_\parallel). \quad (49)$$

We correct the bias factor and apply the Wiener filter to obtain the reconstructed clean field $\hat{\kappa}$ which we use as the estimator of δ ,

$$\hat{\kappa}(k_\perp, k_\parallel) = \frac{\kappa_{3D}(k_\perp, k_\parallel)}{b(k_\perp, k_\parallel)} W(k_\perp, k_\parallel), \quad (50)$$

where

$$W(k_\perp, k_\parallel) = \frac{P_\delta(k_\perp, k_\parallel)}{P_\delta(k_\perp, k_\parallel) + P_n(k_\perp, k_\parallel)/b^2(k_\perp, k_\parallel)}. \quad (51)$$

The real space $\kappa(\mathbf{x})$ can then be obtained by inverse Fourier transform.

IV. SIMULATION

In this section we explore the cosmic tidal reconstruction process in all details using the dark matter density

fields from N -body simulations. Then we discuss the dependence on smoothing scale and the necessity of Gaussianization. At last, we study the anisotropic noise in reconstruction.

We run N -body simulations using the CUBEP³M code [16] with 2048^3 dark matter particles in a box of side length $L = 1.2$ Gpc/ h . We have adopted the following set of cosmological parameter values: $\Omega_b = 0.049$, $\Omega_c = 0.259$, $h = 0.678$, $A_s = 2.139 \times 10^{-9}$ and $n_s = 0.968$. Six runs with independent initial conditions were performed to provide better statistics. In the following calculations we use outputs at $z = 0$.

A. Reconstruction

We follow the simple, slightly sub-optimal scenario in [3]. We first smooth the 3D density field using a Gaussian window function,

$$\bar{\delta}(\mathbf{x}) = \int d^3x' S(\mathbf{x} - \mathbf{x}') \delta(\mathbf{x}'), \quad (52)$$

where $S(\mathbf{r}) = e^{-r^2/2R^2}$. The smoothing scale is $R = 1.25$ Mpc/ h as in Ref.[3]. As will be shown below, the reconstruction result is not sensitive to the smoothing scale until we smooth on linear scales, i.e. $R \gtrsim 5$ Mpc/ h . Then we take a logarithmic transform $\delta_g(\mathbf{x}) = \ln[1 + \bar{\delta}(\mathbf{x})]$ to Gaussianize the density field [11]. The additive constant $\langle \ln(1 + \bar{\delta}(\mathbf{x})) \rangle$ will not affect our reconstruction results, as we only use the derivatives of this field. Next we convolve the log density field $\delta_g(\mathbf{x})$ with the filter $w_i(\mathbf{x})$ in Eq.(37), and then obtain the three dimensional tidal shear fields $\gamma_1(\mathbf{x})$ and $\gamma_2(\mathbf{x})$ using Eq.(38). The two tidal shear fields $\gamma_1(\mathbf{x})$ and $\gamma_2(\mathbf{x})$ directly describe the quadrupolar distortions of the density field in the tangential plane, while the variation of the density field along the z axis is inferred from the variations of the transverse tidal shear fields in the z direction. By combining $\gamma_1(\mathbf{k})$ and $\gamma_2(\mathbf{k})$ using Eq.(43), we obtain the 3D convergence field $\kappa_{3D}(\mathbf{k})$. We estimate $\langle \kappa_{3D} \delta \rangle$ and $\langle \kappa_{3D} \kappa_{3D} \rangle$ using the power spectra from these six simulations and then get $b(k_\perp, k_\parallel)$ and $P_n(k_\perp, k_\parallel)$. We estimate the clean field $\hat{\kappa}(\mathbf{k})$ from Eq.(50).

In Fig. 1, we show a 1.17 Mpc/ h slice of the original density field in the $x-y$ plane in the left panel and a slice of the reconstructed density field in the right panel, both smoothed on 8 Mpc/ h to reduce the small scale noise in order to make visual comparisons. In Fig. 2 we show the similar slices in the $x-z$ plane. We find that in both the $x-y$ and $x-z$ plane, the reconstructed density fields resemble the original ones, demonstrating that the reconstruction works well. However, the strong peaks in the original density field are less prominent in the reconstructed field. The peaks in the original density field correspond to strongly nonlinear structures, like some very massive halos. In deriving Eq.(27), we assume that the small scale density fluctuations undergo linear evolutions and the local anisotropy is due to the long wave-

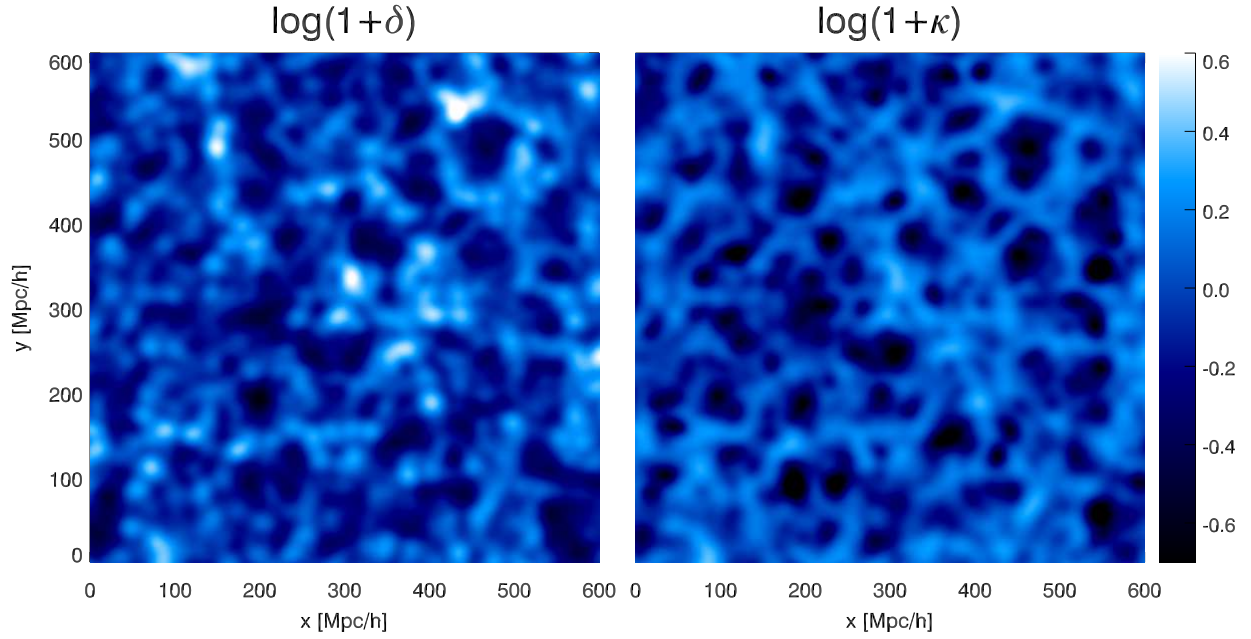


FIG. 1: The left panel shows a slice of the original density field $\delta(\mathbf{x})$ smoothed on $8 \text{ Mpc}/h$ in $x - y$ plane. The right panel shows the corresponding slice of the reconstructed density field $\kappa(\mathbf{x})$, also smoothed on $8 \text{ Mpc}/h$.

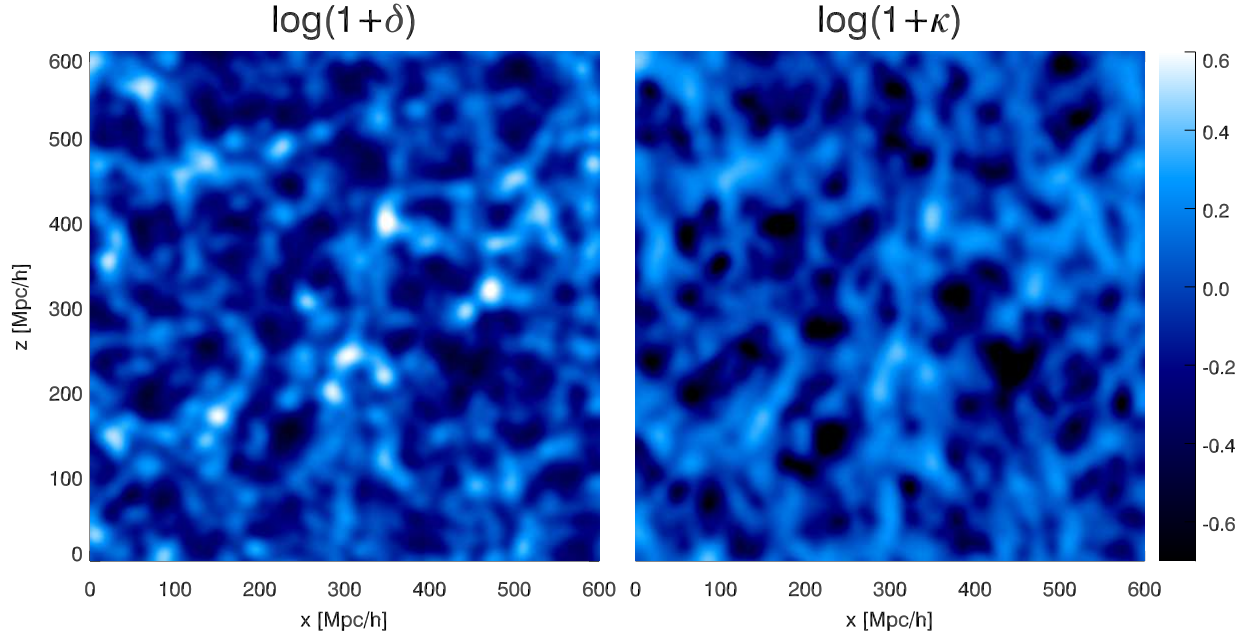


FIG. 2: The left panel shows a slice of the original density field $\delta(\mathbf{x})$ smoothed on $8 \text{ Mpc}/h$ in $x - z$ plane. The right panel shows the corresponding slice of the reconstructed density field $\kappa(\mathbf{x})$, also smoothed on $8 \text{ Mpc}/h$.

length tidal field. However, the self-gravitational interaction is very strong around these nonlinear structures, so they change little under the weak gravitational interaction with the long wavelength tidal field. Eq.(27) does not hold in these regimes. The reconstruction exploits

the nonlinear coupling between the long wavelength tidal field and the small scale density fluctuations, but limited by the strong nonlinear gravitational clustering on small scales during structure formation, which leads to non-Gaussianity. Indeed, the original density field needs to

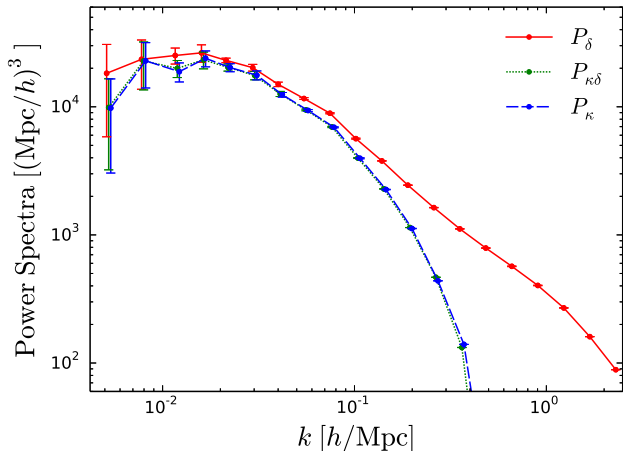


FIG. 3: The auto and cross power spectra of the original and reconstructed density fields.

be smoothed and Gaussianized to reduce the weighting of such contributions in order to obtain good reconstruction results.

In Fig. 3, we show the auto power spectra of the original field δ , the reconstructed field κ and the cross power spectrum between κ and δ . Data points in the same k -bin are shifted slightly for clarity of display. The large errors at $k \sim 0.005 h/\text{Mpc}$ is due to finite modes on the largest scales. However, we see a good cross correlation between the original and reconstructed density fields over a wide range of wavenumbers, $0.008 h/\text{Mpc} \lesssim k \lesssim 0.1 h/\text{Mpc}$. The general shape of P_κ is similar to that of P_δ . The power spectrum for κ and the cross power spectrum between κ and δ are nearly the same in this range because after we apply the Wiener filter to the reconstructed noisy field κ_{3D} , the part correlated with δ remains in the clean field κ . At $k > 0.1 \text{ Mpc}/h$, the auto power spectrum of κ and the cross power spectrum drop more rapidly than the original density field, showing that the reconstruction does not work well on such small scales.

In Fig. 4 we plot the cross correlation coefficient between the original density field and reconstructed density field, $r_{\kappa\delta} \equiv P_{\kappa\delta}/\sqrt{P_\delta P_\kappa}$. The error bars are estimated by the bootstrap resampling method. The cross correlation coefficient $r_{\kappa\delta} > 0.9$ for $0.008 h/\text{Mpc} \lesssim k \lesssim 0.1 h/\text{Mpc}$, confirming our visual impression that the reconstruction produces good results. The cross coefficient drops rapidly at $k > 0.1 \text{ Mpc}/h$ because the reconstruction ceases to work on small scales.

B. Effect of smoothing and Gaussianization

To test how the reconstruction depends on the choice of smoothing scale, we also perform reconstruction with three more smoothing scales, $R = 2.5 \text{ Mpc}/h$, $R = 5 \text{ Mpc}/h$ and $R = 10 \text{ Mpc}/h$, these are also shown in Fig. 4 with different line styles. We see that the cross cor-

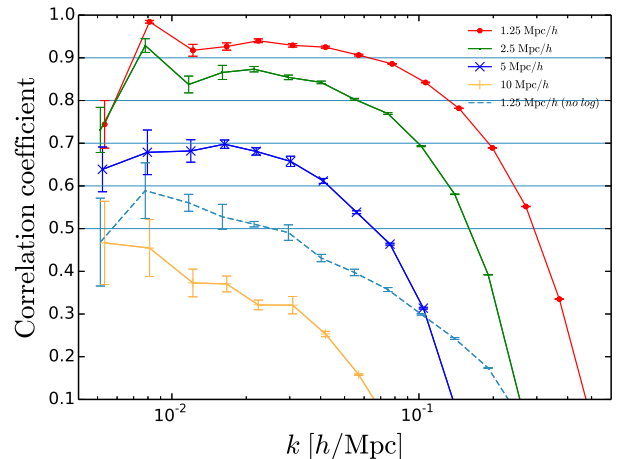


FIG. 4: Cross correlation coefficients for different smoothing scales and the reconstruction without the logarithmic transform.

relation coefficient decreases when the smoothing scales are increased. We are using the small scale structures to reconstruct the large scale density field. With larger smoothing scales, more small scale structures which provide cosmological information about the large scale density field are lost. However, the reconstruction results do not degrade significantly until the smoothing scale goes beyond $5 \text{ Mpc}/h$, roughly the scale on which the structure growth transits from linear to non-linear. Smoothing with larger window sizes will cause so much information loss that the cross correlation coefficients become very small.

The logarithmic transform plays an important role in the cosmic tidal reconstruction. In Fig. 4 we also plot the result for a reconstruction without the logarithmic transform. We find the cross correlation between the reconstructed field and the original field is much weaker than the one with the logarithmic transform, and quickly drops to nearly zero when the wavenumber increases. Apparently, in this case the non-Gaussianity limits the accuracy of the shear reconstruction. The tidal shear estimators derived under the Gaussian assumption are not necessarily optimal for the non-Gaussian density field. The logarithmic transform reduces the non-Gaussianity of the density field and fixes the displacement-density relation significantly as shown in [11], so a much better result can be achieved.

C. The Anisotropic Noise

The error in κ_{3D} is anisotropic as we discussed earlier. We show the anisotropic noise power spectrum in Fig. 5. The noises for modes with large k_\parallel and small k_\perp are orders of magnitude larger than other modes. This result confirms the estimate of noise derived from theory, $\sigma_{\kappa_{3D}}^2 \propto (k^2/k_\perp^2)^2$, which diverges for small k_\perp . In

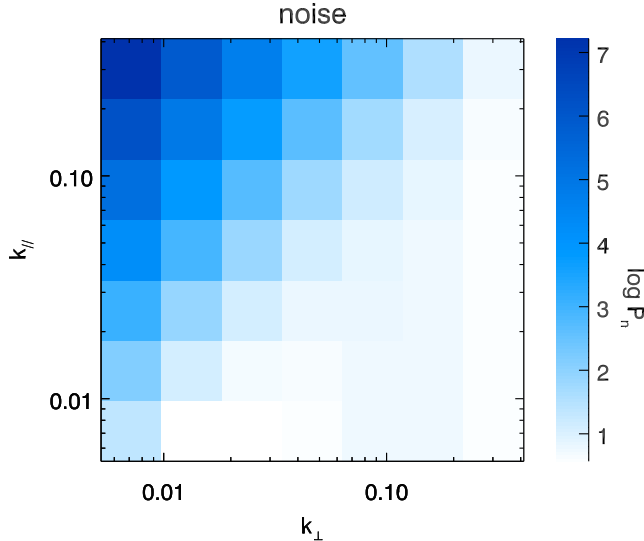


FIG. 5: The anisotropic noise power spectrum $P_n(k_{\parallel}, k_{\perp})$.

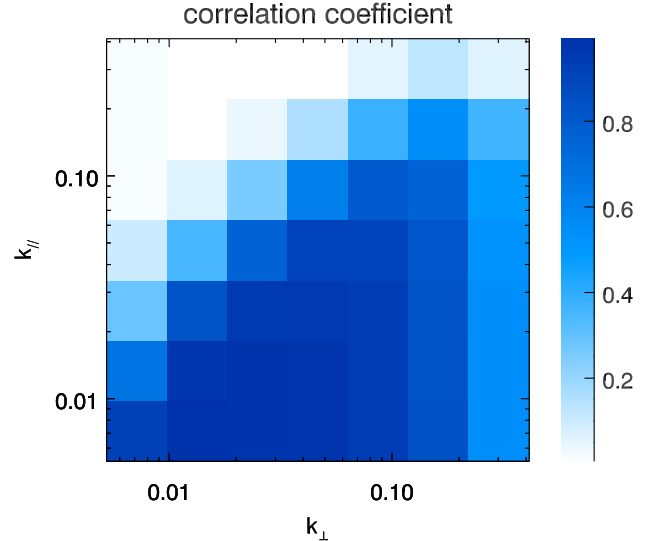


FIG. 6: The anisotropic cross correlation coefficient $r_{\kappa\delta}(k_{\parallel}, k_{\perp})$.

Fig. 6, we show the anisotropic correlation coefficient $r_{\kappa\delta}(k_{\parallel}, k_{\perp}) = P_{\kappa\delta}(k_{\parallel}, k_{\perp}) / \sqrt{P_{\delta}(k_{\parallel}, k_{\perp})P_{\kappa}(k_{\parallel}, k_{\perp})}$. The correlation between the original and reconstructed fields is better at the lower right corner, which can be close to 1 for modes with small k_{\parallel} , but drops quickly when k_{\parallel} increases, the modes with large k_{\parallel} and small k_{\perp} are poorly reconstructed.

In Fig. 7 we show the anisotropic bias factor. The bias factor is nearly constant except for modes with very large k_{\parallel} and very small k_{\perp} , where the cosmic tidal reconstruction is noisy. This constancy of the bias factor shows that our reconstructed density field is a faithful representation of the original density field. It is also encouraging for applying the reconstructed density field to do cross correlations with other tracers for beating down cosmic variances [17].

The anisotropy in reconstruction is due to the fact we only use tidal shear fields in the $x-y$ plane. The changes of the long wavelength density field δ_L along the line of sight are inferred indirectly from the variations of tidal shear fields $\gamma_1(\mathbf{x})$ and $\gamma_2(\mathbf{x})$ along z axis, so we can not capture the rapid changes of the density field along z axis. By including tidal shear fields containing derivatives with respect to z axis, the reconstruction will be improved. However, redshift space distortion will inevitably affect the reconstruction result. We leave the detailed study of this in a future paper.

V. DISCUSSIONS

In this paper we show how the long wavelength tidal field t_{ij} can be reconstructed from the local small scale power spectrum. To reconstruct t_{ij} from the anisotropic small scale density perturbations, we need to learn the interaction process clearly. In this paper, we follow the treatments in [1], only considering the coupling between

\mathbf{s}_{1s} and \mathbf{s}_{1t} , which is the leading order effect from t_{ij} . However, the tidal interaction is inherently a nonlinear process. Higher order terms of form $(\mathbf{s}_{1s})^n \mathbf{s}_{1t}$ ($n > 1$) also play important roles in the tidal interaction, as the nonlinearities on small scales are quite strong. The proportional coefficient in Eq.(28) will change if we include terms like $(\mathbf{s}_{1s})^n \mathbf{s}_{1t}$ ($n > 1$). The tidal shear estimators we used in this paper are biased since we do not know the tidal interaction process accurately. In this paper we assume that the nonlinearities only change the proportional coefficient $f(k, \tau)$. The tidal distortions of the local power spectrum is still proportional to $\hat{k}^i \hat{k}^j t_{ij}^{(0)}$ and the proportional coefficient does not differ the one in Eq.(28) significantly over different wavenumbers. Then we can absorb the unknown coefficient into the bias factor introduced in Eq.(46). The bias factor can be solved from N -body simulations. The proportional constant from the Poisson equation and the normalization constant Q in the tidal shear estimators can also be absorbed in this bias factor. The integral for Q in Eq.(33) would diverge at large k if there were no noise in the power spectrum $P(k)$, i.e. $P(k) = P_{tot}(k)$. This happens when we use the dark matter density field from high precision N -body simulations to reconstruct the large scale density field. The bias factor solves this problem. The result could be improved in the future by including the higher order perturbations. Nevertheless, the reconstruction works well even at this leading order, with the cross correlation coefficient larger than 0.9 until $k \gtrsim 0.1 \text{ Mpc}/h$. The reconstruction should work even better at higher redshifts where the small scale density fluctuations undergo less nonlinear evolutions.

The $\hat{\gamma}_1$ and $\hat{\gamma}_2$ estimators are optimal under the Gaussian assumption, while this is not the real case. The non-Gaussian density field is treated as a Gaussian random field throughout the reconstruction. So we need to Gaussianize the non-Gaussian density field or the correlation

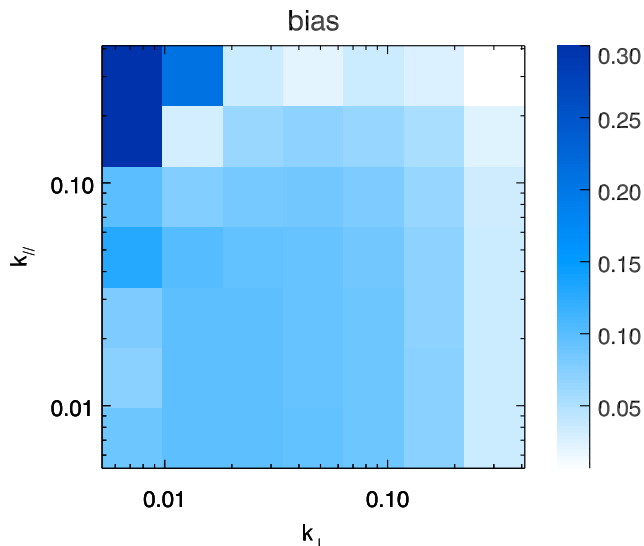


FIG. 7: 2D bias factor $b(k_{\parallel}, k_{\perp})$. The bias factor is almost scale independent in this plane. $b(k_{\parallel}, k_{\perp})$ saturates at the upper left corner. Since these modes are noisy, the extremely large values of the bias at that corner are not reliable.

would be rather weak. It would be worthwhile to investigate the optimal estimators for non-Gaussian sources, which can be constructed from N -body simulations.

There is still one more limitation in the reconstruction. The $\hat{\gamma}_1$ and $\hat{\gamma}_2$ estimators are unbiased and of minimum variance in the long wavelength limit, providing optimal tidal shear reconstructions. However, at larger wavenumbers, the tidal shear field would be underestimated by a scale dependent bias multiplicative factor which needs to be corrected [4, 12]. In this paper, we find the estimator derived in the long wavelength limit still works well if we only use the reconstruction modes with scale larger than the smoothing scale. However, when there is an overlap between these two scales, the reconstruction result would degrade. More sophisticated method is needed in that case.

Here we use the dark matter density field directly to reconstruct the large scale density field. However, the actual tracers would be galaxies, which are located inside dark matter halos which are in turn distributed in

the underlying dark matter density field. Due to the discreteness of the galaxy/halo field, the tidal reconstruction may not be as good as that of the dark matter field. The scale dependent galaxy/halo bias may also complicate the reconstruction procedure. We plan to study this problem in future.

The reconstruction method developed in this paper has great potential applications. The reconstructed field κ gives the distribution of dark matter on large scales. By cross correlating with the original galaxy/halo field, we can measure the logarithmic growth rate without sample variance [18]. This can potentially provide high precision measurements of neutrino masses and tests of gravity. The reconstructed field κ is also important for measuring the dark matter-neutrino cross-correlation dipole [19]. Moreover, it is also important in the case where the measurement of long wavelength modes is missing or has large noise. In the 21cm intensity mapping survey [20], modes with small radial wavenumbers are seriously contaminated by foreground radiation, and are often subtracted in data analysis. This makes it difficult or even impossible to do cross-correlation with surveys which only probe the long wavelength radial mode, including weak lensing, photo- z galaxies, integrated Sachs-Wolf effect and kinetic Sunyaev-Zel'dovich effect. Since cosmic tidal reconstruction can recover the long wavelength radial modes, it enables the cross-correlation of the 21cm intensity survey with other cosmic probes. For 21cm intensity mapping experiments such as Tianlai [21, 22] and CHIME [23], the cosmic tidal reconstruction method can be very useful.

VI. ACKNOWLEDGEMENT

Our simulation computations were performed on the BlueGene/Q supercomputer located at the University of Toronto's SciNet HPC facility. We acknowledge the support of the Chinese MoST 863 program under Grant No. 2012AA121701, the CAS Science Strategic Priority Research Program XDB09000000, the NSFC under Grant No. 11373030, 11473032, and 11403071, IAS at Tsinghua University, CHEP at Peking University, and NSERC.

-
- [1] F. Schmidt, E. Pajer, and M. Zaldarriaga, Phys. Rev. D **89**, 083507 (2014), 1312.5616.
 - [2] Y. Li, W. Hu, and M. Takada, Phys. Rev. D **90**, 103530 (2014), 1408.1081.
 - [3] U.-L. Pen, R. Sheth, J. Harnois-Deraps, X. Chen, and Z. Li, ArXiv e-prints (2012), 1202.5804.
 - [4] T. Lu and U.-L. Pen, MNRAS **388**, 1819 (2008), 0710.1108.
 - [5] T. Lu, U.-L. Pen, and O. Doré, Phys. Rev. D **81**, 123015 (2010), 0905.0499.
 - [6] S. R. Furlanetto and A. Lidz, ApJ **660**, 1030 (2007), astro-ph/0611274.
 - [7] P. J. Adshead and S. R. Furlanetto, MNRAS **384**, 291 (2008), 0706.3220.
 - [8] M. F. Morales, B. Hazelton, I. Sullivan, and A. Beardsley, ApJ **752**, 137 (2012), 1202.3830.
 - [9] K. W. Masui and U.-L. Pen, Physical Review Letters **105**, 161302 (2010), 1006.4181.
 - [10] D. Jeong and M. Kamionkowski, Physical Review Letters **108**, 251301 (2012), 1203.0302.
 - [11] B. L. Falck, M. C. Neyrinck, M. A. Aragon-Calvo, G. Lavaux, and A. S. Szalay, ApJ **745**, 17 (2012), 1111.4466.
 - [12] M. Bucher, C. S. Carvalho, K. Moodley, and M. Re-

- mazeilles, Phys. Rev. D **85**, 043016 (2012), 1004.3285.
- [13] D. M. Eardley, D. L. Lee, A. P. Lightman, R. V. Wagner, and C. M. Will, Physical Review Letters **30**, 884 (1973).
 - [14] N. Kaiser and G. Squires, ApJ **404**, 441 (1993).
 - [15] M. Zaldarriaga and U. Seljak, Phys. Rev. D **59**, 123507 (1999), astro-ph/9810257.
 - [16] J. Harnois-Déraps, U.-L. Pen, I. T. Iliev, H. Merz, J. D. Emberson, and V. Desjacques, MNRAS **436**, 540 (2013), 1208.5098.
 - [17] U. Seljak, Physical Review Letters **102**, 021302 (2009), 0807.1770.
 - [18] P. McDonald and U. Seljak, J. Cosmology Astropart. Phys. **10**, 007 (2009), 0810.0323.
 - [19] H.-M. Zhu, U.-L. Pen, X. Chen, D. Inman, and Y. Yu, Physical Review Letters **113**, 131301 (2014), 1311.3422.
 - [20] T.-C. Chang, U.-L. Pen, J. B. Peterson, and P. McDonald, Physical Review Letters **100**, 091303 (2008), 0709.3672.
 - [21] X. Chen, International Journal of Modern Physics Conference Series **12**, 256 (2012), 1212.6278.
 - [22] Y. Xu, X. Wang, and X. Chen, ApJ **798**, 40 (2015), 1410.7794.
 - [23] K. Bandura, G. E. Addison, M. Amiri, J. R. Bond, D. Campbell-Wilson, L. Connor, J.-F. Cliche, G. Davis, M. Deng, N. Denman, et al., in *Society of Photo-Optical Instrumentation Engineers (SPIE) Conference Series* (2014), vol. 9145 of *Society of Photo-Optical Instrumentation Engineers (SPIE) Conference Series*, p. 22, 1406.2288.